A Solar-Powered Hand-Launchable UAV for Low-Altitude Multi-Day Continuous Flight

Philipp Oettershagen[1], Amir Melzer, Thomas Mantel, Konrad Rudin,
Rainer Lotz, Dieter Siebenmann, Stefan Leutenegger, Kostas Alexis and Roland Siegwart

***Abstract*— This paper presents the conceptual design, detailed development and flight testing of *AtlantikSolar*, a 5.6m-wingspan solar-powered Low-Altitude Long-Endurance (LALE) Unmanned Aerial Vehicle (UAV) designed and built at ETH Zurich. The UAV is required to provide perpetual endurance at a geographic latitude of 45°N in a 4-month window centered around June 21st. An improved conceptual design method is presented and applied to maximize the perpetual flight robustness with respect to local meteorological disturbances such as clouds or winds. Airframe, avionics hardware, state estimation and control method development for autonomous flight operations are described. Flight test results include a 12-hour flight relying solely on batteries to replicate night-flight conditions. In addition, we present flight results from Search-And-Rescue field trials where a camera and processing pod were mounted on the aircraft to create high-fidelity 3D-maps of a simulated disaster area.**

I. INTRODUCTION

When carefully designed, solar-electrically powered fixed-wing Unmanned Aerial Vehicles (UAVs) exhibit significantly increased flight endurance over purely-electrically or even gas-powered aerial vehicles. Given suitable environmental conditions, a solar-powered UAV stores excess solar energy gathered during the day in its batteries, which may then power the aircraft through the night and, potentially, subsequent day-night cycles. Long-endurance capability, especially in the extreme form of continuous multi-day flight, or *perpetual endurance*, is particularly interesting for applications such as large-scale mapping, observation, or telecommunication relay. Such functionalities may be applied to Search-And-Rescue (SAR) missions, industrial or agricultural inspection, meteorological surveys, border patrol and more [1].

Recently, interest in employing large-scale (wingspan above 20m), solar-powered High-Altitude Long-Endurance (HALE) UAVs as *atmospheric satellites* - i.e. stationary/loitering platforms e.g. for telecommunications relay - has peaked. Notable examples of this trend are *Solara* [2] and *Zephyr*, the latter of which has already demonstrated a continuous flight of 14 days [3]. In contrast, smaller scale solar-powered UAVs are mostly designed for Low-Altitude Long-Endurance (LALE) applications. Though faced with more challenging meteorological phenomena in the lower atmosphere (clouds, rain, wind gusts or thermals), low-altitude UAVs provide the advantages of higher resolution imaging with reduced cloud obstruction, lower complexity and cost and simplified handling (e.g. through hand-launchability). These traits are highly beneficial for first-aid SAR scenarios as well as other inspection tasks. Research targeting perpetual endurance in small-scale solar UAVs has been relatively sparse, with most research focusing on conceptual design studies without extensive flight experience, e.g. [4]. However, Cocconi's *SoLong* [5] performed a continuous 48-hour flight using solar power while actively seeking out thermal updrafts, though with limited airplane autonomy. Noth presents the conceptual design methods, realization and experimental flight results of the 3.2m wingspan *Sky-Sailor* [6], which demonstrated a 27-hour solar-powered continuous flight without the use of thermals in 2008.

This paper aims to extend the work of [5], [6] by presenting *AtlantikSolar* (Figure 1), a solar-powered LALE-UAV designed for robust multi-day autonomous operation while providing the option to use an advanced optical and infrared sensor system together with on-board computation resources. The complete development cycle from conceptual UAV design to actual testing and missions will be presented, or more specifically

(a) the application and extension of the conceptual design approach in [6], [7] towards robust perpetual endurance flight under sub-optimal meteorological conditions,
(b) the realization of the conceptual design in UAV hardware, i.e. structure, low-level electronics & avionics,
(c) the development of on–board state estimation algorithms

Fig. 1. The *AtlantikSolar* solar-powered UAV developed at ETH Zurich

All authors are part of the Autonomous Systems Lab, Swiss Federal Institute of Technology Zurich (ETH Zurich). Leonhardstrasse 21, 8092 Zurich, Switzerland.

[1] E-Mail:philipp.oettershagen@mavt.ethz.ch

*This work was supported by the EU-FP7 research projects ICARUS and SHERPA as well as a number of project partners and generous individuals, see http://www.atlantiksolar.ethz.ch/

and flight control methods based on an Extended Kalman Filter (EKF) and PID control with non-linear guidance and

(d) the discussion of flight test results including long-endurance flight (up to 12 hours) and mapping during exemplary SAR missions.

II. CONCEPTUAL DESIGN METHODOLOGY

The conceptual design methodology for solar-powered UAVs used in this paper relies on the work in [6], [7]. It is extended to include uncertainty in local meteorological conditions such as clouds or winds.

A. System Model

The general approach for perpetual endurance for LALE-UAVs is to fly level at low altitude to be energy–efficient, while charging the batteries. When the batteries are fully charged, the excess energy is used to climb and gain potential energy. To analyze flight performance the energy input/output-balance under the assumption of level flight at lowest admissible altitude is modeled. The total required nominal electric output power

$$P_{out}^{nom} = \frac{P_{level}}{\eta_{prop}} + P_{av} + P_{pld} \tag{1}$$

consists of the required electric propulsion power for level-flight $\frac{P_{level}}{\eta_{prop}}$, where η_{prop} includes propeller, gearbox, motor, and motor-controller efficiency, and the necessary avionics and payload power P_{av} and P_{pld}. The UAV is assumed to fly at the airspeed of minimum aerodynamic level-flight power

$$P_{level} = \left(\frac{C_D}{C_L^{\frac{3}{2}}}\right)_{min} \sqrt{\frac{2(m_{tot}g)^3}{\rho(h)A_{wing}}}. \tag{2}$$

Here, $m_{tot} = m_{bat} + m_{struct} + m_{prop} + m_{sm} + m_{av} + m_{pld}$ is the total airplane mass, where structure, propulsion and solar module masses m_{struct}, m_{prop}, m_{sm} are optimized and m_{av}, m_{pld} are given in Table I. The local earth gravity is designated by g, A_{wing} is the wing area, and $\rho(h)$ is the altitude dependent air density. The airplane lift and drag coefficients C_L and C_D are retrieved from 2-D airfoil simulations using XFoil [8], with C_D being combined with parasitic drag from the airplane fuselage and stabilizers and the induced drag

$$C_{D,ind} = \frac{C_L^2}{\pi \cdot e_0 \cdot \lambda}. \tag{3}$$

Here, $e_0 \approx 0.92$ is the Oswald efficiency and λ the wing aspect ratio. On the input side, the nominal solar input power

$$P_{solar}^{nom} = I \cdot A_{sm} \cdot \eta_{sm} \cdot \eta_{mppt} \tag{4}$$

considers the solar module area $A_{sm} = f_{sm} \cdot A_{wing}$ with relative fill-factor f_{sm}, module efficiency η_{sm}, and Maximum Power Point Tracker (MPPT) efficiency η_{mppt}. The solar radiation $I = I(\varphi, h, t)$ is assumed to be a function of the geographical latitude φ, the altitude h, and the current date and local time t, and is modeled as in [9]. While the batteries are not fully charged ($E_{bat} < E_{bat}^{max}$), the energy balance may be written as

$$\frac{dE_{bat}}{dt} = P_{solar}(\varphi, h, t) - P_{prop} - P_{av} - P_{pld}. \tag{5}$$

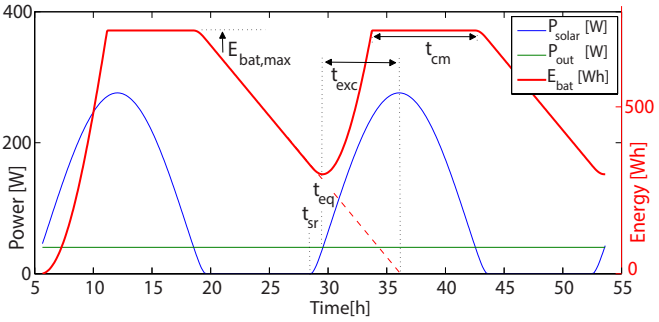

Fig. 2. Exemplary energetic simulation of the *AtlantikSolar* UAV configuration ($b = 5.6m$, $\lambda = 18.5$, $m_{bat} = 3.5kg$), showing input and output power, battery capacity, performance metrics excess time t_{exc} and charge margin t_{cm} during a 2-day flight.

Here, P_{prop} is the current electric power sent to the propulsion system. Further, the altitude state equation is given by

$$\frac{dh}{dt} = \frac{\eta_{prop} \cdot P_{prop} - P_{level}(h)}{m_{tot} g}. \tag{6}$$

Integration of the differential equations (5) and (6) finally allows to analyze the energy stored in the batteries and thus the perpetual flight capability of the UAV.

For the design optimization, we assume that a solar-powered UAV configuration is designed for missions at and around a specific Date of the Year (DoY) and geographical latitude φ, thus φ and DoY are fixed. The three design parameters are a) wingspan b and b) wing aspect ratio λ, which both specify wing geometry and thus influence level-power (2) and solar input power (4), and c) the battery mass m_{bat} contained in m_{tot} in (2).

B. Extension of Conceptual Design Optimization Criteria

The conceptual design tool developed in [6], [7] has been extended in two ways: First, it now provides the capability to perform energetic simulations of multi-day solar-powered flight, whereas before only one day-night cycle was considered. Figure 2 shows the results for incoming solar power P_{solar}, required power P_{out}, and remaining battery charge E_{bat} obtained for a flight of two subsequent day-night cycles. Clearly, the initial charge condition E_{bat} at time of sunrise $t_{sr} = \min(t(P_{solar} > 0))$ for the second day is different than on the first day, which significantly influences the re-charging process. Second, and more importantly, the optimization criteria are extended to achieve a more robust multi-day flight. In general, a necessary and sufficient condition for perpetual flight is that the excess time $t_{exc} > 0$, where

$$t_{exc} = \left.\frac{E_{bat}(t = t_{eq})}{P_{out}^{nom}}\right|_{P_{solar}(t > t_{sr}) = 0} \tag{7}$$

with *power-equality time* $t_{eq} = t(P_{solar}^{nom} = P_{out}^{nom})$ in the morning. This means that remaining battery capacity has to exist at $t = t_{eq}$ to continue flight for instance in case of cloud coverage. Therefore, the authors in [6], [7] focus on maximizing t_{exc}. However, a large t_{exc} does not provide direct robustness against disturbances in P_{solar} e.g. due to cloud cover during the charging process. In contrast, when

optimizing purely for t_{exc}, the methodology in Sec. II-A will select the largest battery size (due to the scaling of P_{level} with m_{bat}) which can be fully charged under optimal conditions, but every reduction in P_{solar} will directly decrease t_{exc} due to only partially charged batteries. Thus, we introduce the charge margin t_{cm} as the time margin between achieving the full charge $E_{bat} = E_{bat}^{max}$ and restart of the discharge in the evening. In case of decreased solar power income, $t_{cm} > 0$ provides additional margin before a decrease in excess time occurs.

The overall approach for increasing robustness with respect to local power disturbances is thus to determine the lowest acceptable t_{exc} satisfying the UAV application requirements, and then to optimize the configuration for t_{cm}. The exact procedure applied in this paper is:

1. Selection of nominal operating latitude φ, Day of Operation DoY^{nom} and the outermost days where perpetual UAV endurance is required $DoY^{\min,\max}$
2. Retrieval of the night durations $t_{night}^{\min}$, $t_{night}^{\max}$ from [9] for the range of $DoY = [DoY^{\min}, DoY^{\max}]$
3. The required excess time t_{exc}^{req} is now the sum of
   - $t_{exc,DoY} = t_{night}^{max} - t_{night}^{min}$
   - $t_{exc,clouds}$, to allow a margin for clouds in the morning or evening
   - $t_{exc,P_{level}}$, to allow a margin for increased power consumption e.g. caused by downdrafts or uncertainties in estimating P_{level}
4. Design analysis given the methodology in Section II-A for $DoY(t_{night} = t_{night}^{min})$. Pre-selection of the subset $\mathcal{S}$ of configurations satisfying $t_{exc} > t_{exc}^{req}$
5. Allowance for a set of intermediate configurations $\mathcal{S}_i$ within $\mathcal{S}$ while taking UAV-specific constraints on b, λ, or m_{bat} into account. Selection of the final configuration $\mathcal{S}_f$ from $\mathcal{S}_i$ in order to obtain the largest charge margin t_{cm}

This conceptual design methodology is applied below. An alternative conceptual design approach utilizing a weighted version of t_{exc} and t_{cm} is proposed in [4].

C. Application of Conceptual Design Methodology

AtlantikSolar operates at a nominal latitude of $\varphi = 45°N$ and shall provide perpetual endurance within a +/-2 month window centered around DoY^{nom}=June 21st (April 21st-August 21st). From [9], we find $t_{night}^{min} = 8.7h$ (June 21st), $t_{night}^{max} = 10.5h$ (April 21st), and thus $t_{exc,DoY} = 1.80h$. We choose $t_{exc,clouds} = 3.0h$ to account for three hours of full cloud coverage either on the evening or the morning and choose $t_{exc,P_{level}} = 0.2 \cdot t_{night}^{max} = 2.1h$ to cover increased power consumption due to modeling errors, downdrafts or headwinds. Using $t_{exc}^{req} = t_{exc,DoY} + t_{exc,clouds} + t_{exc,P_{level}}$, we retrieve $t_{exc}^{req} = 6.9h$ as the minimum required excess time for robust perpetual flight at the given dates and locations.

The design methodology tool of Section II-A is now applied assuming the fixed parameters in Table I. Figure 3 shows the resulting plot for t_{exc} versus the optimization

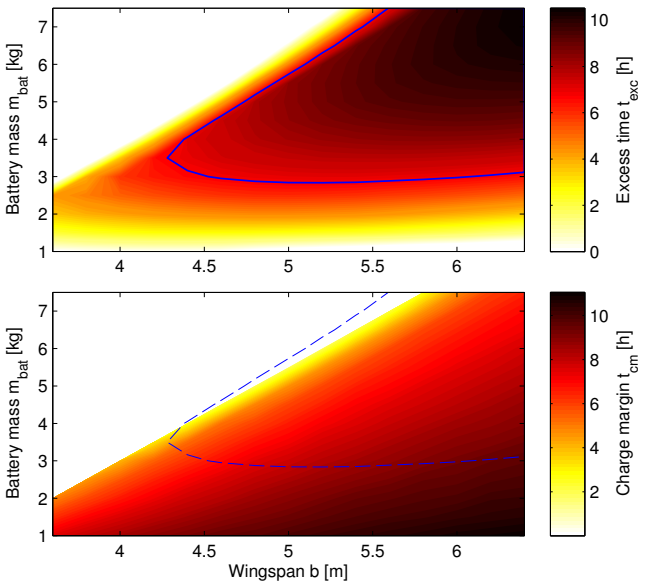

Fig. 3. Excess time t_{exc} (top) and charge margin t_{cm} (bottom) vs. b and m_{bat}, all at $\lambda = 18.5$. The configuration subset $\mathcal{S}$ satisfying $t_{exc} > t_{exc}^{req}$ under our design requirements lies inside the blue contour line.

variables b and m_{bat}. The subset $\mathcal{S}$ of configurations satisfying $t_{exc} > t_{exc}^{req}$ is the region within the blue contour-line. The optimum clearly occurs at large wingspans. However, considering that we aim for a small-scale and hand-launchable configuration that allows easy transportation (in this case via disassembly of the main wing into three pieces of less than $2m$ wingspan) we choose $b = 5.6m$. The aspect ratio $\lambda = 18.5$ is found to provide an optimum in t_{exc} and also allows to seamlessly integrate the 125mm-wide solar cells (see Section III-A.1) inside the wing chord. The last design choice is m_{bat}, for which we seek to optimize t_{cm} within the previously selected set $\mathcal{S}_i = (\mathcal{S}|_{b=5.6m,\lambda=18.5})$. As visible in Figure 3, $m_{bat} = 3.0...7.5kg$ lies within $\mathcal{S}_i$. We choose $m_{bat} = 3.5kg$ to optimize t_{cm} and due to practical battery sizing constraints described in Section III-A.1. The selected final configuration $\mathcal{S}_f = (\mathcal{S}|_{m_{bat}=3.5kg,b=5.6m,\lambda=18.5})$ yields an estimated $m_{tot} = 7.22kg$, $t_{exc} = 7.89h$ and $t_{cm} = 8.38h$ for the nominal operating date and latitude.

TABLE I

FIXED PARAMETERS FOR THE CONCEPTUAL DESIGN

Parameter	Value	Description
η_{sm}	0.20	Solar module efficiency
η_{MPPT}	0.95	MPPT efficiency
η_{prop}	0.58	Propulsion system efficiency
e_{bat}	874800J/kg	Battery specific energy
f_{sm}	0.94	Solar module fill factor
k_{sm}	0.59kg/m^2	Solar module areal density
m_{av}	0.6kg	Avionics mass (including all cabling)
m_{pld}	0.1kg	Payload mass
P_{av}	4.5W	Avionics power consumption
P_{pld}	0.0W	Payload power consumption

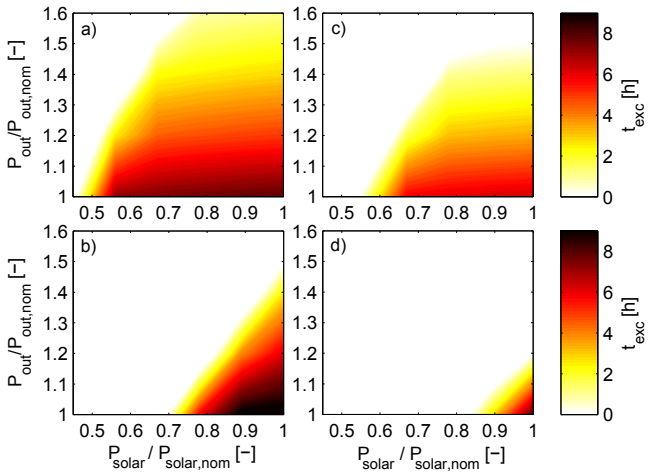

Fig. 4. Excess time under disturbed power input and output for the $b = 5.6m$, $\lambda = 18.5$ configuration: a) m_{bat}=3.5kg on June 21st b) $m_{bat} = 6.0kg$ on June 21st c) m_{bat}=3.5kg on April 21st d) $m_{bat} = 6.0kg$ on April 21st

D. Robustness Analysis

To verify the multi-day flight robustness of the developed UAV configuration, we analyze its performance considering a set of local disturbances in UAV power input and output, namely

(a) The disturbed solar power income P_{solar}^{dist}, as caused by clouds or fog. Lacking knowledge of the exact spatial and temporal disturbance distribution, we assume

$$P_{solar}^{dist}(t) = P_{solar}^{nom}(t) \cdot k_{CCF}. \tag{8}$$

Here, $k_{CCF} \in [0,1]$ represents the current cloud cover factor [10], i.e. the clearness of the atmosphere.

(b) The disturbed electric power output P_{out}^{dist}. Wind downdrafts, head wind, or gusts may require increased propulsion or actuation power. Again, we assume

$$P_{out}^{dist}(t) = P_{out}^{nom}(t) \cdot k_{OPF} \tag{9}$$

with k_{OPF} representing the Output Power Factor.

Figure 4 shows the remaining excess time with respect to these disturbances. The UAV configuration developed in Section II-C ($m_{bat} = 3.5kg$) still provides perpetual endurance with less than 50% of the solar power income or if more than 60% increased power are required on June 21st (Figure 4a). In contrast, a configuration purely optimized towards excess time ($m_{bat} = 6.0kg$, Figure 4b) will yield a higher maximum t_{exc} of 9.5h, but the robustness with respect to clouds or higher required level power is greatly decreased. On April 21st, the UAV configuration of Section II-C still provides solid robustness (Figure 4c), which verifies the $DoY^{nom} \pm$ 2 months perpetual endurance requirement. In contrast, the $m_{bat} = 6.0kg$ configuration (Figure 4d) cannot provide reliable perpetual endurance anymore. Overall, the configuration developed using the extended optimization criteria from Section II-B thus shows significantly improved multi-day flight robustness in comparison with configurations that are purely optimized for maximum excess time.

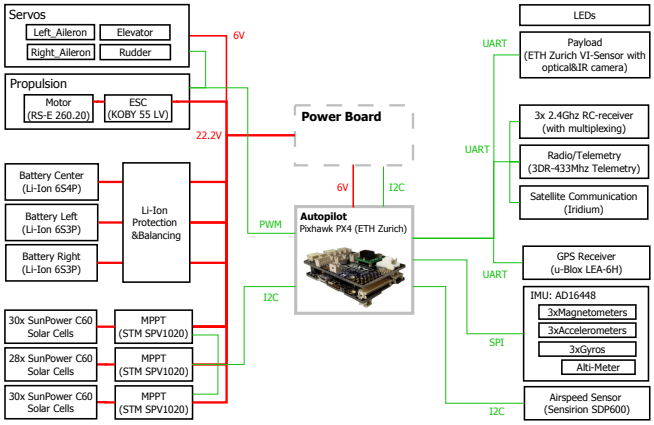

Fig. 5. AtlantikSolar system overview. For clarity, voltage lines from the autopilot to connected devices (5.0V and 3.3V) are omitted.

III. DETAILED DESIGN AND REALIZATION

Although the design of *AtlantikSolar* is mostly dictated by the requirement for low level-flight power consumption, it provides means to mount an advanced optical and infrared sensor pod for use in autonomous search and rescue or industrial inspection missions. An overview over the airplane system topology is given in Figure 5 and the airplane airframe characteristics are summarized in Table II.

TABLE II
ATLANTIKSOLAR DESIGN CHARACTERISTICS

Parameter	Value
Wing span	5.65m
Wing chord	0.305m
Length	2.03m
Height	0.45m
Total mass*	7.36kg
Battery mass	3.52kg
Max. payload mass	0.8kg
Wing loading	4.28kg/m^2
Stall speed	8.1m/s

*With batteries, no payload

A. UAV Platform Design

1) Airframe: The wing and stabilizers of *AtlantikSolar* are built in a traditional rib-spar construction method (Figure 6). The wing's main element is an inner cylindrical carbon-fiber spar to resist torsional wing loads. Four carbon-fiber belts of trapezoidal and laterally-varying cross-section are attached to the spar to optimally resist bending loads and to provide maximum wing stiffness to avoid bending of the solar cells. The main wing can be disassembled into three wing pieces of less than 2m each.

2) Energy Generation and Storage: The cylindrical wing spars are fitted with 72 cylindrical high energy density Lithium-Ion batteries (Panasonic NCR18650b, 243Wh/kg) to optimally distribute the mass in a *span loader* concept. The cells are connected in a 6S (21.6V) configuration and

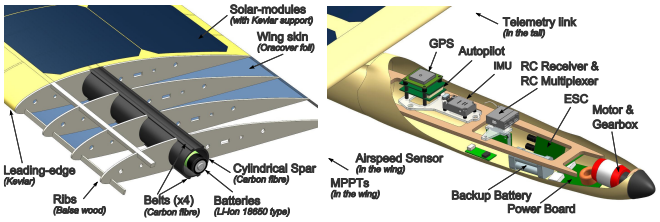

Fig. 6. Left: Wing structure with integrated batteries and solar cells. Right: Main avionics layout inside the airplane.

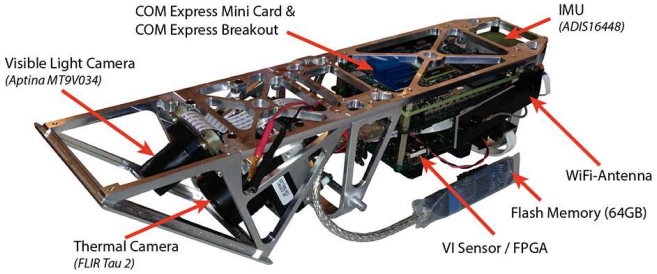

Fig. 7. Sensing and processing unit for integration below the wing.

provide $E_{bat}^{max} = 850Wh$ at $m_{bat} = 3.5kg$. The solar modules feature a total of 88 SunPower C60 cells with $\eta_{sm} = 0.20$, an areal density of $k_{sm} = 590g/m^2$ and a maximum power output of 275W at $\varphi = 45°$N on June 21st. Modules featuring SunPower E60 cells with $\eta_{sm} = 0.23$ are currently being integrated [11]. The solar modules are seamlessly embedded in the upper wing surface to avoid premature flow separation.

3) Actuation: The propulsion system features a foldable custom built carbon-fiber propeller with diameter $D = 0.66$m and pitch $H = 0.60$m. It is driven by a 5:1 reduction-ratio planetary gearbox, a RS-E Strecker 260.20 brushless DC motor with $k_V = 400RPM/V$ and a Kontronik Koby 55 LV motor controller at up to $P_{prop}^{max} = 450W$ electric input power. The actuation system consists of four Volz DA-15N servos that drive the two ailerons, the all-moving elevator and the rudder. In order to assess the reliability of the actuation system over a multi-day flight, the Volz actuators were successfully operated in a servo test-bed for 30 days under flight-equivalent loads [12].

4) Avionics: The avionics installation (Figures 5 and 6) is centered around a Pixhawk PX4 Autopilot - an open source and open hardware project initiated at ETH Zurich - with a Cortex M4F microprocessor running at 168MHz and featuring 192kB RAM. For attitude estimation (Section III-B.1), an ADIS16448 10-Degrees of Freedom (DoF) Inertial Measurement Unit (IMU), a u-blox LEA-6H GPS receiver, and a Sensirion SDP600 differential pressure sensor are used. The SDP600 airspeed sensor exhibits less than 5% error at airspeed of 8m/s, which is essential to closely track the power-optimal airspeed v_{air}^{opt}. Both a 433MHz medium-range telemetry link and a long-range IRIDIUM-based satellite backup link are integrated. The airplane implements a fully manual RC-command fall-back mode in case of a severe autopilot failure. Night operations are possible due to four on-board high-power indicator LEDs.

5) Payload: The capabilities of AtlantikSolar are augmented by a sensor and processing unit (Figure 7) which may be mounted beneath the wing. It incorporates a *visual-inertial sensor system* [13] and a small form factor computer based on an Intel Atom processor. The former consists of an ARM-FPGA system, an ADIS16448 IMU as well as two cameras - a FLIR Tau 2 for Long-Wavelength Infrared (LWIR) and an Aptina MT9V034 for visible light imaging - and allows accurate real-time SLAM [14]. The latter is intended for high-level path planning and equipped with WiFi-communication to transmit a video feed to the ground.

B. State Estimation and Control Design

1) State Estimation: The on-board state estimator is based on an EKF design that fuses data from the 10-DoF IMU, GPS and airspeed sensor as described in Section III-A.4. It is implemented and optimized in order to grant full functionality on the microcontroller-based autopilot and offers a robust estimation solution that can cope with prolonged GPS outage scenarios by compensating through airspeed measurements. Successive estimations of the position, velocity, orientation (attitude and heading), QFF (pressure at sea level), gyroscope biases, accelerometer biases and the wind vector are rendered, with sideslip angle and Angle of Attack (AoA) being subsequently derived from these estimates. A detailed description and verification of the state estimator functionality can be found in [15].

2) System Identification: Towards aiding the control synthesis procedure, a simplified linear state–space representation of the UAV dynamics was also derived based on recorded flight data and frequency–domain system identification methods. For approximately level flight, linear models may capture the vehicle response for small perturbations around a given equilibrium. Decoupling the longitudinal and lateral axis, the dynamics of a UAV may take the form presented in [16] and used in the authors previous work [17]. Within this work, the exact aforementioned lateral dynamics representation is employed. The longitudinal dynamics are extended to account for the effect of throttle and are expressed as

$$\begin{aligned} \mathbf{M}_{lon}\dot{\hat{\mathbf{x}}}_{lon} &= \mathbf{A}'_{lon}\hat{\mathbf{x}}_{lon} + \mathbf{B}'_{lon}\mathbf{u}_{lon} \\ \hat{\mathbf{x}}_{lon} &= \begin{bmatrix}\hat{u} & \hat{w} & \hat{q} & \hat{\theta}\end{bmatrix}^T \end{aligned} \tag{10}$$

where $\hat{u}, \hat{w}, \hat{q}, \theta$ correspond to the predicted body x–, z–axis velocities, the pitch rate and the pitch angle, respectively. $\mathbf{u}_{lon} = [u_{Elev}\ u_{Throt}]^T$ corresponds to the elevator deflection and the throttle command, respectively. In

$$\begin{aligned} \mathbf{M}_{lon} &= \begin{bmatrix} m_{tot} & 0 & 0 & 0 \\ 0 & m_{tot} & 0 & 0 \\ 0 & 0 & I_y & 0 \\ 0 & 0 & 0 & 1 \end{bmatrix}, \ \mathbf{B}'_{lon} = \begin{bmatrix} X_{u_{elev}} & X_{u_{throt}} \\ Z_{u_{elev}} & Z_{u_{throt}} \\ M_{u_{elev}} & M_{u_{throt}} \\ 0 & 0 \end{bmatrix} \\ \mathbf{A}'_{lon} &= \begin{bmatrix} X_u & X_w & X_q - m_{tot}W_e & -m_{tot}g\cos\theta_e \\ Z_u & Z_w & Z_q + m_{tot}U_e & -m_{tot}g\sin\theta_e \\ M_u & M_w & M_q & 0 \\ 0 & 0 & 1 & 0 \end{bmatrix} \end{aligned} \tag{11}$$

W_e, U_e, θ_e are the trimming points of u, w, θ and the elements of $\mathbf{M}_{lon}, \mathbf{A}'_{lon}$ and $\mathbf{B}'_{lon}$ form the stability and control derivatives of the longitudinal dynamics.

The employed frequency–domain system identification framework is based on the objective function and guidelines outlined in [18] and its specifics were further detailed in our previous work [17]. Employing the same methods, models of sufficient fidelity were derived for the *AtlantikSolar* UAV as shown in Figure 8, while the increased coherence values indicate that the linearity assumption within such a subset of the flight envelope is effectively correct. Results of similar quality are also derived for the case of the lateral dynamics.

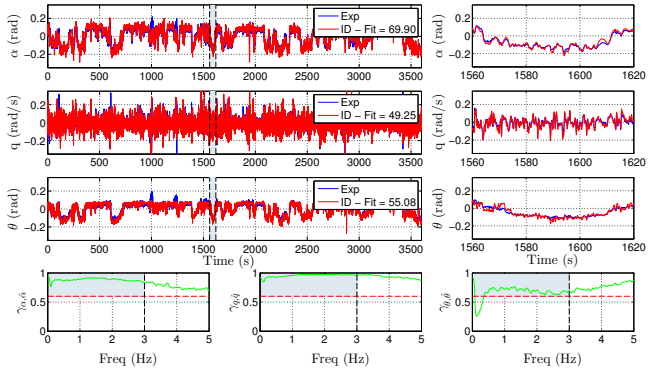

Fig. 8. Longitudinal dynamics system identification validation. The AoA α is computed based on the experimental and model–predicted values for u and w. Results for 1h are shown along with a closer look to 60sec of the flight and the coherence values γ between the experimental α, q, θ and the predicted $\hat{\alpha}, \hat{q}, \hat{\theta}$.

3) Control: AtlantikSolar features autonomous navigation up to the level of loitering through user–defined waypoints. The complete control structure (Figure 9) is tuned offline based on the identified system model (Sec. III-B.2), functionality is tested in an X–Plane 10 Hardware–In–the–Loop (HIL) simulation and finally refined in extensive flight tests. For inner–loop control, our baseline–solution corresponds to a set of cascaded saturated PID controllers: the Stability Augmentation System (SAS) applies rate–damping to shape the airplane's frequency response, while the Control Augmentation System (CAS) applies proportional–integral feedback to achieve roll (ϕ) and pitch (θ) reference tracking. Furthermore, flight tests showed that due to AtlantikSolar's high aspect ratio and thus high inertia (I_z and I_x especially), coordinated turn control is essential to smoothen the adverse yaw behaviour and achieve the no–sideslip yaw rate $r = \frac{g \cdot \sin(\phi)}{v_{air}}$. To avoid overload of the highly optimized structure, output limiters are applied. Additionally, the control actions are in a final stage adapted with respect to the dynamic pressure $q = \frac{1}{2}\rho v_{air}^2$ which accounts for the change of the effective moments created by the control surfaces.

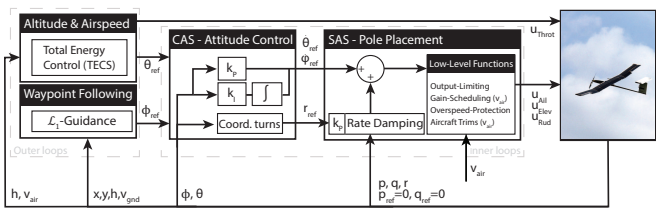

Fig. 9. Control Scheme implemented for *AtlantikSolar*.

Once the inner–loops are well–tuned, waypoint guidance is enabled. *AtlantikSolar* employs a $\mathcal{L}_1$–nonlinear guidance law which generates the lateral acceleration reference $a_{s_{ref}}$ and corresponding roll references ϕ_{ref} of the UAV based on a look–ahead distance L_1 and the current ground speed and heading as detailed in [19] along with the online adaptation of the look–ahead distance as in [20]. This guidance law is integrated into our control structure as described in [17] and combined with an extended version of the Pixhawk open–source Total Energy Control System (TECS) [21] which provides altitude control: First, a slew rate constraint on the reference altitude h_{ref} has been integrated to reach smoother altitude control at pre-definable climb and sink rates, which is especially important for low propulsion-power to weight ratio UAVs such as *AtlantikSolar*. Second, thermal compliance has been implemented to cope with up- and downdrafts. In an updraft, the standard TECS implementation will decrease the pitch reference θ_{ref} to decrease the altitude if $h > h_{ref}$. Instead of actively working against thermals, we allow the UAV to gain potential energy from an updraft: TECS is altered such that θ_{ref} is fully and only used for airspeed control and u_{Throt} only for altitude control. When at $h > h_{ref}$, the plane will thus keep $\theta_{ref} = \theta_{ref}(t)$ such that $v_{air}(t) = v_{air,ref}(t)$ and will gradually reduce motor power, potentially gaining altitude for strong thermals. Furthermore, hard constraints have been implemented, i.e. full throttle is forced for $h < h_{min}$, at $h > h_{max}$ we gradually allow a pitch-down and thus altitude decrease again, and at $h > h_{max} + 50m$ the controller automatically engages the spoilers for maximum descend rate. The inner PID-based pitch- and roll control loops are executed at a sampling period of $T_{SAS,CAS} = 0.01s$, while the high-level $\mathcal{L}_1$&TECS controllers run with $T_{\mathcal{L}_1,TECS} = 0.05s$. Given these settings, the full controller requires less than 4% CPU load, 5KB of RAM and 47KB Flash memory and is thus computationally lightweight when compared to other Pixhawk applications (see [17]). The whole controller is designed to be modular, and more sophisticated approaches like model predictive control [17] and robust H_∞–based controllers [22] have been implemented and flown for evaluation on test planes in addition to the aforementioned PID–baseline inner–loop control solution.

IV. EXPERIMENTAL RESULTS

A total of 85 hours of flight testing have been performed in 49 flights with the two *AtlantikSolar* UAVs designed and built so far. The following section briefly summarizes the main results required and obtained for efficient long-endurance flight and application of the platform in Search-And-Rescue missions.

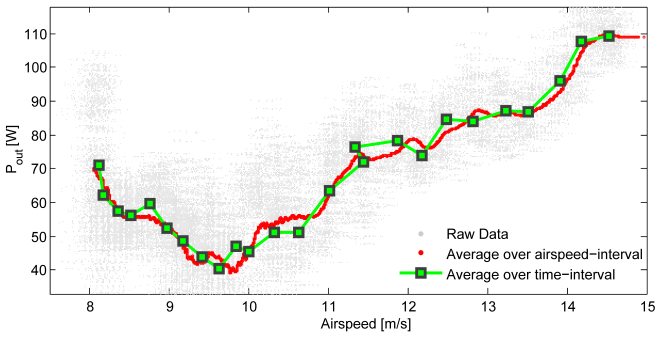

Fig. 10. *Power curve*, i.e. the total required level power P_{out} vs. airspeed, measured in constant-altitude loiter mode with $v_{air,ref} = const = 8...15m/s$ in $T = 200s$ intervals. (a) Raw data, (b) P_{out} averaged over 1000 neighboring airspeed data points and (c) P_{out} averaged within the $T = 200s$ intervals.

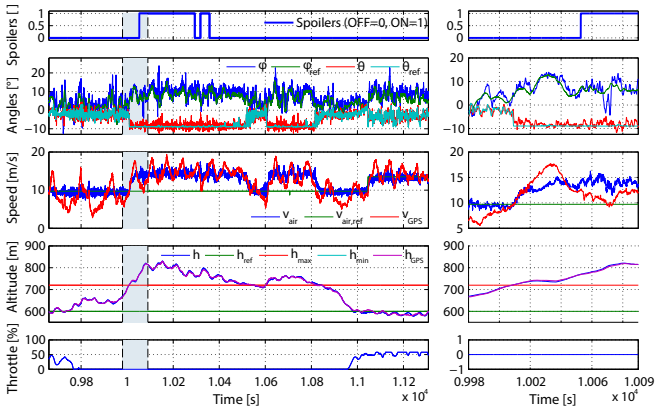

Fig. 11. Fully autonomous flight in constant altitude-reference loitering mode under the influence of significant thermal updrafts and winds. Left: The autopilot engages spoilers and motor as required to respect altitude limits h_{min} and h_{max} in its thermal compliance mode. Right: A zoomed-in section of the left plot gives insight into attitude reference tracking.

A. Subsystem Level Test Results

1) Measurement of required level flight power: To verify the energetic UAV modeling in Section II-A, constant-altitude loitering flights performed in calm air were used to record the power curve (Figure 10) for *AtlantikSolar*. Although a significant portion of noise remains, it can be stated that $P_{out}^{min} \approx 42...48W$ at $v_{air}^{opt} = 9.7 \pm 0.5m/s$. The modeling through (1)-(3) yielded $P_{out} = 44.5W$ for *AtlantikSolar*. This correspondence means that - on the output power side - the predicted 24-hour flight capability and excess time are verified. However, it should be noted that the low power consumption from Figure 10 was only reached after significant re-iterations on propeller, motor and motor-controller design through wind-tunnel and lab tests. In general, the modeling through (1)-(3) is an absolute lower limit for power consumption as it assumes undisturbed flight at minimum sink airspeed, whereas in reality deviations in airspeed and attitude or even downdrafts cannot be avoided.

2) Autopilot operation in challenging wind conditions: Challenging wind conditions strain a UAV's state estimation and control capabilities. A segment from a fully autonomous verification flight of *AtlantikSolar* under such conditions is

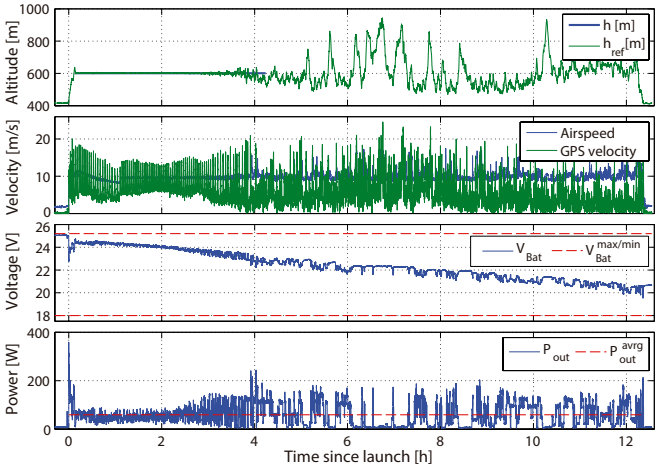

Fig. 12. A 12h 22min flight performed by *AtlantikSolar* to test the endurance under night-flight conditions, i.e. without solar power income. The red-dotted lines are (a) the battery voltage at maximum/minimum state-of-charge in the voltage plot and (b) the mean of the output power (59W) over the whole flight in the power plot.

shown in Figure 11. The aircraft is in constant altitude-reference loiter mode, and after hitting a thermal at $t = 9760s$ it correctly switches off the motor, keeps θ_{ref} due to the implemented thermal compliance (Section III-B.3) and thus gains altitude. When the altitude is above the user-prescribed h_{max}, negative pitch reference is prescribed and successfully tracked. The aircraft however continues to gain altitude due to the significant updraft strength. From $t = 10052s$ on, the autopilot thus engages the spoilers at $h > h_{max} + 50$m to achieve maximum descent rate. The aircraft's altitude begins to stabilize and the spoilers are disengaged at $t = 10357s$. After a total of 20 minutes of unpowered flight, the altitude stabilizes around $h = h_{ref}$ again, with the controller now commanding high throttle due to the following downdraft.

B. Continuous 12-hour Flight

As a first step towards demonstrating multi-day flights, *AtlantikSolar* performed a 12 hour 22 minutes (276km ground distance) flight under replicated night-conditions (Figure 12), i.e. with the solar power system completely disabled. After launch at 7.15am ($t = 0h$), the UAV performs autonomous constant-altitude loitering to execute the power measurements of Section IV-A.1 and switched to autopilot-assisted (SAS&CAS) modes for additional testing at $t = 4.1h$. The whole flight is marked by severe thermal down- and updrafts with altitude gains up to 350m, with the significant difference between airspeed and GPS-velocity showing horizontal winds on the order of the airspeed (up to 11m/s) for $t > 4h$. Although the average power consumption of 59W is higher than determined in Section IV-A.1, the batteries still show a remaining State of Charge (SoC) of 23% (corresponding to V_{bat}=20.6V) after landing. Extrapolation using the remaining SoC shows that flight times of $t_{endurance} = 15h$ (and even more in calmer conditions) are possible solely on batteries. Crossing the night for the full operating range defined in Section II-C and involving $t_{night}^{max} = 10.5h$ on April 21st thus

seems possible with excess times of $t_{exc} > 4.5h$. This supports the findings of the conceptual design.

C. Mapping Flights in Search and Rescue Scenarios

The AtlantikSolar UAV is utilized within several research projects. Within that framework, it recently participated in the ICARUS project [23] field–trials that took place in Marche–en–Famenne, Belgium. During these trials, several of the UAV's capabilities - including its autonomous long–term operation as required by the SAR teams for collecting aerial data that can be utilized for mapping and reconnaissance purposes - were presented. The sensor pod described in Section III was used to record pose–annotated grayscale images. Furthermore, a GPS–tagged Sony HDR-AS100VW camera was carried on–board. The UAV executed several pre–planned missions ensuring the complete coverage of a given map with its sensors and, with the help of the Pix4D software [24], the pose–annotated images enabled the dense reconstruction of 3D models of the area. Figure 13 presents such results, the reference waypoints and their radius of acceptance along with the recorded flight path and sectors of the dense point clouds.

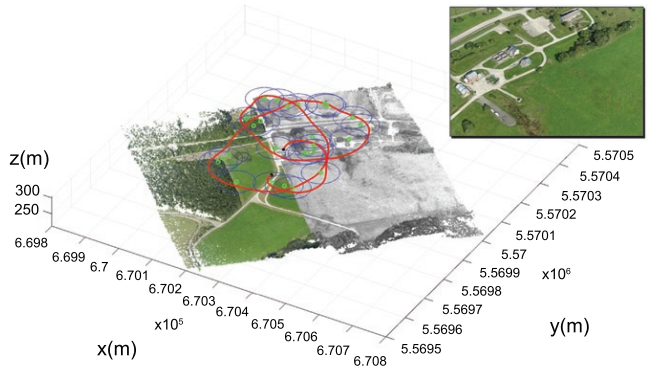

Fig. 13. Inspection mission reference waypoints and recorded path along with dense point clouds of sectors of the 3D reconstruction using the Aptina grayscale camera and the Sony RGB camera. The derived maps come with geoinformation in UTM31N while a small amount of highly–accurate ground control points (GCPs) can improve the georeferencing accuracy.

V. CONCLUSIONS

This paper presented the design, realization and flight testing of a solar-powered hand-launchable LALE UAV for robust (with respect to meteorological disturbances such as clouds) multi-day flight at 45°N geographical latitude from April 21st to August 21st. In-flight power measurements and a 12h 22min flight, powered solely by batteries, confirm the expected endurance and hence that flights through the night are possible. Achievement of these performance results became possible through the thorough application of the presented extended conceptual design methodology along with significant engineering effort, especially with respect to improving flight efficiency. Based upon the developed UAV platform, the next steps are to demonstrate one and multiple day-night (24h/48h) flights. Along with continued long-endurance research, more effort will be put into advanced online localization, map reconstruction and planning capabilities in the existing optical and infrared camera pod to increase the autonomy in the SAR projects that the platform is involved in.

REFERENCES

[1] N. Colella and G. Wenneker, "Pathfinder: developing a solar rechargeable aircraft," *IEEE Potentials*, vol. 15, no. 1, pp. 18–23, 1996.

[2] E. Ackerman, *Giant Solar-Powered UAVs are Atmospheric Satellites*, IEEE Spectrum, 2013.

[3] QinetiQ, *QinetiQ files for three world records for its Zephyr Solar powered UAV*, QinetiQ Press Release, 2010.

[4] S. Morton, L. Scharber, and N. Papanikolopoulos, "Solar Powered Unmanned Aerial Vehicle for Continuous Flight: Conceptual Overview and Optimization," in *IEEE International Conference on Robotics and Automation (ICRA)*, 2013.

[5] A. Cocconi, "AC Propulsion's solar electric powered SoLong UAV," AC Propulsion, Tech. Rep., 2005.

[6] A. Noth, "Design of solar powered airplanes for continuous flight," PhD thesis, ETH Zurich, 2008.

[7] S. Leutenegger and M. Jabas, "Solar airplane conceptual design and performance estimation," *Journal of Intelligent Robot Systems*, vol. 61, pp. 545–561, 2010.

[8] M. Drela, "XFOIL 6.9 User Primer," MIT Aero&Astro, Tech. Rep., 2001.

[9] J. A. Duffie and W. A. Beckman, *Solar Engineering of Thermal Processes*, 3rd. Wiley, 2006.

[10] K. Kimura and D. Stephenson, "Solar radiation on cloudy days," National Research Council of Canada, Tech. Rep., 1969.

[11] J. Sunier, C. Schlumpf, V.Chapuis, P. Oettershagen, R. Siegwart, C. Ballif, and L.-E. Perret-Aebi, *Innovative PV modules for Atlantic Ocean Crossing*, Poster, 2014.

[12] L. DellaCa, "Load Modeling and Reliability Analysis for Actuators on solar powered UAVs," Bachelor thesis, ETH Zurich, 2013.

[13] J. Nikolic, J. Rehder, M. Burri, P. Gohl, S. Leutenegger, P. T. Furgale, and R. Y. Siegwart, "A Synchronized Visual-Inertial Sensor System with FPGA Pre-Processing for Accurate Real-Time SLAM," in *IEEE International Conference on Robotics and Automation (ICRA)*, 2014.

[14] S. Leutenegger, "Unmanned solar airplanes: design and algorithms for efficient and robust autonomous operation," PhD thesis, ETH Zurich, 2014.

[15] S. Leutenegger, A. Melzer, K. Alexis, and R. Siegwart, "Robust state estimation for small unmanned airplanes," in *IEEE Multiconference on Systems and Control*.

[16] A. Dorobantu, A Murch, B. Mettler, and G Balas, "Frequency domain system identification for a small, low-cost, fixed-wing uav," in *Proceedings of the 2011 AIAA Guidance, Navigation, and Control Conference*, 2011.

[17] P. Oettershagen, A. Melzer, S. Leutenegger, K. Alexis, and R. Siegwart, "Explicit Model Predictive Control and $\mathscr{L}_1$-Navigation Strategies for Fixed-Wing UAV Path Tracking," in *22nd Mediterranean Conference on Control & Automation (MED)*, 2014.

[18] Mark B. Tischler, Robert K. Remple, *Aircraft and Rotorcraft System Identification: Engineering methods with Flight-Test examples*. American Institute of Aeronautics and Astronautics (AIAA).

[19] S. Park, J. Deyst, and J. P. How, "A new nonlinear guidance logic for trajectory tracking," in *AIAA Guidance, Navigation, and Control Conference and Exhibit*, 2004, pp. 16–19.

[20] S. Park, J. Deyst and J. P. How, "Performance and lyapunov stability of a nonlinear path following guidance method," *Journal of Guidance, Control, and Dynamics*, vol. 30, no. 6, 2007.

[21] *Pixhawk Autopilot website*.

[22] L. Mosimann, "Robust Fixed Wing Control against Actuator Faults," Master's thesis, ETH Zurich, 2014.

[23] ICARUS: Unmanned Search and Rescue, *http://www.fp7-icarus.eu/*.

[24] Pix4D, *http://pix4d.com/*.